International Journal of Nanomedicine

Dovepress
open access to scientific and medical research

Open Access Full Text Article

ORIGINAL RESEARCH

Mechanism of enhanced antiosteoporosis effect of circinal–icaritin by self-assembled nanomicelles in vivo with suet oil and sodium deoxycholate

This article was published in the following Dove Press journal:
International Journal of Nanomedicine
25 March 2015
Number of times this article has been viewed

Jun Jiang[1,2]
Jie Li[1,2]
Zhenhai Zhang[1,2]
E Sun[1,2]
Liang Feng[1,2]
Xiaobin Jia[1,2]

[1]Key Laboratory of New Drug Delivery System of Chinese Materia Medica, Jiangsu Provincial Academy of Chinese Medicine, [2]College of Pharmacy, Nanjing University of Chinese Medicine, Nanjing, People's Republic of China

Background: Circinal–icaritin (CIT), one new active aglycone of *Epimedium*, can exert a beneficial effect on osteoporotic bone. However, its low bioavailability limits its clinical efficacy for the treatment of osteoporosis.

Materials and methods: In this paper, suet oil (SO) was used to improve the oral bioavailability of CIT and enhance its antiosteoporosis effect and absorption. After oral administration of CIT together with SO, the CIT and SO self-assembled into nanomicelles under the action of sodium deoxycholate (DOC) by bile secretion. The antiosteoporosis effects of the CIT-SO-DOC nanomicelles were evaluated in osteoporotic rats by bone mineral density, serum biochemical markers, bone microarchitecture, bone biomechanical properties, and related protein and gene expressions. We examined the bioavailability of CIT and its nanomicelles in vivo, and subsequently the nanomicelles were verified using transmission electron microscopy. Finally, we evaluated absorption across a rat intestinal perfusion model.

Results: Compared with CIT, in the CIT-SO groups, protein and messenger ribonucleic acid expressions of osteoprotegerin were increased, while expressions of receptor activator of nuclear factor-κB ligand in bone tissue were decreased; bone-turnover markers in serum of hydroxyproline, alkaline phosphatase, tartrate-resistant acid phosphatase 5b, and receptor activator of nuclear factor-κB ligand levels were decreased, while osteoprotegerin and osteocalcin levels were increased; and trabecular bone mass, microarchitecture, and bone biomechanical strength were enhanced. The relative bioavailabilities of CIT-SO high dosage, CIT-SO medium dosage, and CIT-SO low dosage (area under concentration–time curve $[AUC]_{0-\infty}$) compared with that of raw CIT high dosage, CIT medium dosage, and CIT low dosage ($AUC_{0-\infty}$) were 127%, 121%, and 134%, respectively. The average particle size of CIT-DOC was significantly decreased after adding SO ($P<0.01$), and the intestinal permeability coefficients of CIT-SO-DOC nanomicelles in the duodenum, jejunum, ileum, and colon were all significantly improved ($P<0.01$).

Conclusion: The increased antiosteoporosis effects and bioavailability of CIT-SO-DOC self-assembled nanomicelles were due to an increase in absorption of CIT by reducing the particle sizes of CIT. SO may be a practical oral carrier for antiosteoporosis drugs with low bioavailability.

Keywords: circinal–icaritin (CIT), nanomicelles, antiosteoporosis effect, bioavailability, intestinal absorption

Correspondence: Xiaobin Jia
College of Pharmacy, Nanjing University of Chinese Medicine, 138 Xianlin Avenue, Qixia, Nanjing, Jiangsu 210023, People's Republic of China
Tel +86 25 8563 7809
Email xiaobinjia_nj@126.com

Introduction

Epimedium has been frequently prescribed for osteoporotic patients in the People's Republic of China (PRC) for a long time.[1–3] Among *Epimedium*-derived flavonoids, aglycone (icaritin) contains the potential to treat osteoporosis in postmenopausal women

without adverse reactions on reproductive tissues.[4,5] However, circinal–icaritin (CIT; 3,5-dihydroxy-2-[4-methoxy-phenyl]-8,8-dimethyl-9,10-dihydro-8*H*-pyrano[2,3-*f*]chromen-4-one) was the isomeric aglycone of IT, which was first discovered and obtained in our laboratory, and had better antiosteoporosis effects than IT.[6]

Suet oil (SO), which was obtained from *Capra hircus* Linnaeus or *Ovis aries* Linnaeus, contains abundant fatty acids.[7] In clinical practice, SO has been used as an excipient for the processing of the traditional Chinese medicine *Epimedium* for thousands of years, and it has been recorded that SO enhances the invigorant and antiosteoporosis effects of *Epimedium*.[8–10]

In the procedure of oral absorption, the inherent bile acids or their salts have hydrophilic surfaces and a hydrophobic surfaces, which are natural biosurfactants.[11–13] Bile acids or their salts form nanomicelles with fatty acids as drug carriers, which promote drug absorption.[14,15] The fatty acids in SO have long chains and surface activity, which can form self-assembled nanomicelles together with bile salts in the body.[16–20]

Our previous study found that the addition of SO improved biopharmaceutical properties and promoted the absorption of IT by self-assembled nanomicelles in vivo with sodium deoxycholate (DOC).[7] Therefore, in order to improve the bioavailability and the antiosteoporosis effects of CIT, SO was used to prepare CIT, and DOC was used to represent one of the main bile salts. Subsequently, the antiosteoporotic activity between CIT and CIT-SO on the bone metabolism of ovariectomized (OVX) osteoporotic rats was compared by bone mineral density (BMD),[21] bone microarchitecture, bone biomechanical properties, and related protein and gene expressions. Simultaneously, serum biochemical parameters, including serum hydroxyproline (HOP), alkaline phosphatase (ALP), osteoprotegerin (OPG), osteocalcin (OCN), receptor activator of nuclear factor-κB ligand (RANKL), and tartrate-resistant acid phosphatase 5b (TRACP-5b) were detected.

Moreover, in order to further explain the synergistic mechanism of SO, the preparation and characterization of CIT-SO-DOC nanomicelles was simulated in vitro. Then, the size distribution and intestinal permeability coefficient (P*eff) of CIT-DOC and CIT-SO-DOC were evaluated. Finally, this study improved the bioavailability and the antiosteoporosis effects of CIT, and investigated the possible enhancing mechanism of SO on CIT.

Materials and methods

Materials

The drugs used in this study included estradiol valerate (EV; Progynova, Bayer AG, Leverkusen, Germany) and SO, which were commercially available. CIT (purity >98.3%) was prepared by ourselves in our laboratory. The structure of CIT is shown in Figure 1. Hanks' balanced salt solution was acquired from Sigma-Aldrich (USA). DOC was purchased from Sinopharm Chemical Reagent (PRC). Chloral hydrate (Sinopharm) was used as an anesthetic. Experimental water was derived from Milli-Q water (EMD Millipore, USA) throughout this study. Chromatographic-grade methanol and acetonitrile were purchased from Merck (Germany). The other reagents were analytical grade.

Animals

Animal experiments were executed according to the *Guide for the Care and Use of Laboratory Animals*, and were approved by the Animal Ethics Committee of Jiangsu Provincial Academy of Chinese Medicine. All animals was anesthetized with an intraperitoneal injection of 300 mg/kg chloral hydrate, and all efforts were made to minimize suffering. EV, CIT, CIT-SO, and SO were suspended in 0.5% sodium

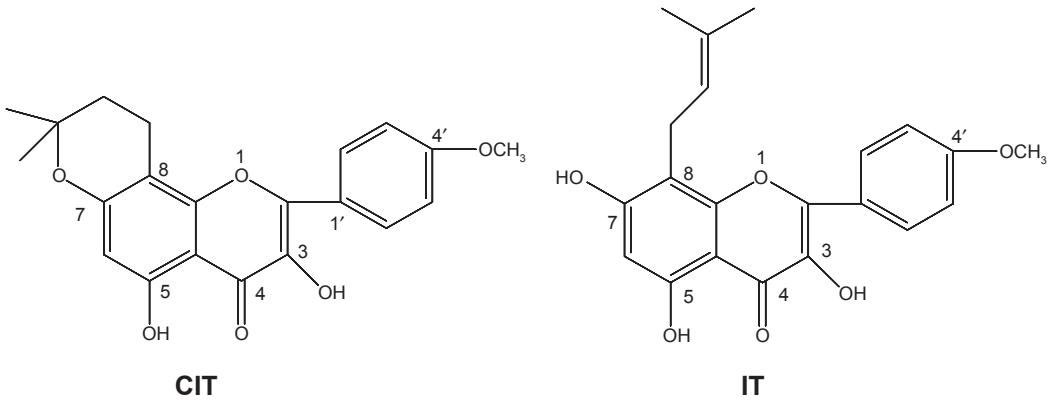

Figure 1 Chemical structures of CIT and IT.
Abbreviation: CIT, circinal–icaritin.

carboxymethyl cellulose and administrated orally. The concentrations of EV, CIT high dosage (CIT-H), CIT medium dosage (CIT-M), and CIT low dosage (CIT-L) were 30 μg/mL, 12 mg/mL, 6 mg/mL, and 3 mg/mL, respectively.

Eighty-four 6-month-old female Sprague Dawley (SLAC Lab Animal Center, PRC) rats (280±20 g) were allowed to adapt to the new environment for 14 days before the experiment. Every four rats were kept in one cage with a standard laboratory rodent diet (calcium content 0.5%) in a suitable indoor environment (25°C, 55% humidity, and 12 hours of day and night alternating). After 14 days of acclimatization, the rats were anesthetized and then bilateral ovaries were examined (sham, n=8) or removed (OVX, n=76). The surgical procedures were done under sterile conditions. Rats were then kept untreated to let them recover and develop osteopenia for 4 weeks.[22] After 28 days, the OVX rats were randomly divided into ten groups, as follows: treated with SO (n=8, 8 mg/kg body weight/day), treated with EV (n=8, 100 μg/kg body weight/day), OVX treated with vehicle (n=8), with CIT-H (n=8, 40 mg/kg body weight/day), with CIT-M (n=8, 20 mg/kg body weight/day), with CIT-L (n=8, 10 mg/kg body weight/day), with CIT-SO-H (n=8, 40 mg/kg body weight/day), with CIT-SO-M (n=8, 20 mg/kg body weight/day), and with CIT-SO-L (n=8, 10 mg/kg body weight/day), which ran from week 5 (day 29) after OVX to week 16 (day 112). The remaining OVX (n=4) rats were used for intestinal absorption experiments. Body weight was monitored once a week, and SO, EV, and CIT dose were adjusted according to their body weight. Oral administration was adopted for all groups of rats. After 12 weeks of treatment, all rats were anesthetized, and their blood was taken from the carotid artery and allowed to clot, followed by being centrifuged at 3,000 *g* for 10 minutes. Rat sera were collected and stored at −20°C until biochemical assays. Then, femur weight and uterus wet weight were recorded after removing their adherent connective tissues. Right femurs were prepared to detect BMD, and then scanned by micro-computed tomography (micro-CT), followed by Western blot assays. Left femurs were used for quantifying gene expression by real-time polymerase chain reaction (PCR). Right tibias were estimated by the three-point bending test.

Bone mineral-density testing

The right total femur was used to measure BMD by dual energy X-ray absorption spectrometry (Hologic, USA) coupled with software (edition 13.1.2) under the small-animal scan mode. BMD results are presented as milligram of mineral contents per square centimeter of surface area.

Biomechanical evaluation

The fresh right tibias were isolated and evaluated for biomechanical testing[23] by a CSS-4420 material-testing machine (Changchun Research Institute for Testing Machines, PRC). Force and displacement data were automatically collected, and the load-deformation curve was drawn subsequently. The measurements of energy to yield point (mJ), extrinsic stiffness (N/mm) and ultimate load (N) were calculated from the load-deformation curve.

Trabecular bone-structure testing

The right distal femurs from each group were scanned by a micro-CT system (eXplore Locus; GE Healthcare, PRC) with version MicroView ABA. The scanning parameter was set at 80 W, with an isotropic voxel size of 22 μm. Bone volume over total volume (BV/TV), trabecular number (TbN), trabecular separation (TbSp), trabecular thickness (TbTh), bone mineral content (BMC), tissue mineral content (TMC), tissue mineral density (TMD), calibration of trabecular separation – 3-D (CalibTbSp3D), calibration of trabecular thickness – 3-D (CalibTbTh3D), and volume of bone (VOB) were obtained as bone morphometric parameters from volume-of-interest (VOI) analysis.

Bone-turnover markers in serum

HOP (A030-2) and ALP (A059-1) were determined by commercial assay kits (Nanjing Jiancheng Bioengineering Institute, PRC). The levels of OPG (R046-2), OCN (R035), RANKL (R085-2), and TRACP-5b (R052-2) were measured by corresponding enzyme-linked immunosorbent assay (ELISA) kits (Nanjing Jiancheng Bioengineering Institute, Nanjing, PRC).

HOP is the main component of collagen, which is the main component of connective tissue. When large amounts of connective tissues are destroyed, such as osteoporosis, this can cause an increase in serum HOP content.[24] Serum ALP is mainly secreted by osteoblasts. A high serum ALP level indicates a bone disease, which may be osteoporosis.[25] OPG is an osteoclast-inhibitory factor and inhibits osteoclast function. Postmenopausal estrogen deficiency leads to an increase in osteoclast activity and bone resorption, which manifests as a decrease in serum OPG level.[26] Serum OCN is synthesized and secreted by OCN, which may reflect the activity of osteoblasts. In the process of postmenopausal osteoporosis, OCN can significantly increase.[27] After menopause, serum TRACP-5b significantly increases, due to ovarian dysfunction and the reduction of endogenous estrogen. Subsequently, bone resorption is greater than bone formation, and the incidence of

osteoporosis is increased.[28] Many metabolic bone diseases are due to an imbalance of bone formation between the resorption of osteoclast bone and remodeling of osteoblastic bone. RANKL is an essential adjustment factor of osteoclast proliferation, differentiation, activation, and survival.[29]

Western blot assays

Right femurs were homogenized using a tissue homogenizer (PowerGen model 1000; Thermo Fisher Scientific, USA) after the addition of 400 μL lysate. The resultant mixture was centrifuged (13,000 *g*) for 10 minutes at 4°C. Supernatants were collected and packed for protein assay (Pierce BCA; Thermo Fisher Scientific). Equal amounts of protein (40 μg) were then diluted by sample buffer (1.0 mol/L Tris-HCl, pH 6.8, 10% [v/v] glycerol, 10% sodium dodecyl sulfate, 0.1% bromophenol blue), and run in 10% sodium dodecyl sulfate polyacrylamide gel-electrophoresis gels. Samples were transferred into nitrocellulose membranes by electroblotting (BioRad, PRC). Filters were blocked for 2 hours in a blocking buffer containing 5% powdered milk and Tris-buffered saline +0.1% Tween. Filters were then incubated with a primary antibody – OPG (1:1,000) or RANKL (1:1,000) – at 4°C overnight. After being washed four times (10 minutes each), membranes were incubated for 2 hours with secondary antibodies (Nanjing KeyGen Biotech, PRC). The bands were developed by enhanced chemiluminescence using LumiGlo (Cell Signaling Technology, USA). The detection process was carried out by gel imager. Quantification was achieved by digitizing the blots using an imaging station and then measuring band density.

Real-time PCR

The tissue homogenizer (PowerGen model 1000) and TRI reagent were used to extract total ribonucleic acid (RNA) from left femurs. Then, a random hexamer was used to convert total RNA into complementary deoxyribonucleic acid by reverse transcriptase (high-capacity complementary deoxyribonucleic acid reverse-transcription kit; Applied Biosystems, USA). Gene-specific PCR primers and gene-specific Taqman probes (Applied Biosystems) were used to complete real-time PCR amplification. The PCR mixture was run in a MultiGene Gradient TC9600-G System (Labnet, USA). The relative OPG and RANKL gene expressions were normalized to the expression of glyceraldehyde 3-phosphate dehydrogenase.

Preparation and characterization of CIT-SO-DOC micelles

CIT-SO-DOC self-assembled nanomicelles were prepared by stirring and mixing at 400 rpm for 4 hours after adding CIT (3.4 mg), SO (0.7 mg), and DOC (7.5 mg) into Hanks' balanced salt-solution buffer (500 mL, pH 7.4). A Zetasizer Nano ZS (Malvern Instruments, UK) was used to determine the size distributions of the CIT self-assembled nanomicelles. Transmission electron microscopy (TEM; JEM-1200EX; JEOL, Japan) was applied to evaluate the morphology.

Intestinal absorption of CIT-SO-DOC micelles

After a fast of 12 hours, the small intestines of rats were exposed by cutting along the ventral midline followed by being anesthetized. The intestinal content of the duodenum, upper jejunum, terminal ileum, and colon was rinsed slowly with physiological saline. Each bowel had one entrance-and-exit nylon tube, which was secured by ligation with silk suture. During the surgery, each bowel was carefully monitored to avoid kinks and ensure a consistent flow direction (from the duodenum to the ileum). Open body cavities were covered by saline-soaked cotton to prevent loss of fluids.[30] The perfusate constant was kept warm at 37°C with inlet cannulas and circulating water baths. The perfusate samples were collected every 30 minutes, with a flow rate of 0.2 mL/min. The concentration of CIT in the effluent was determined by ultraperformance liquid chromatography tandem mass spectrometry (UPLC-MS/MS).

Pharmacokinetics of CIT and CIT-SO after oral administration

Pharmacokinetic studies were carried out by dividing the rats into six groups (CIT-H, CIT-M, CIT-L, CIT-SO-H, CIT-SO-M, and CIT-SO-L), with three rats in each group. After the administration of CIT and CIT-SO to the rats through oral gavage, blood samples were gathered from the eye ground vein and then transferred into heparinized tubes at time points of 1, 2, 4, 6, 8, 10, 12, 14, 16, 24, and 36 hours. Plasma samples (100 μL) were used and spiked successively with 20 μL of 2 M sodium acetate buffer (pH 4.5) and 20 μL of 0.2 M sodium acetate buffer (pH 4.5) containing β-glucuronidase/sulfatase at concentrations of 9,000/500 units/mL. After incubation for 60 minutes at 37°C for enzyme-hydrolysis treatment, and then vortexing for 5 minutes, 10 μL of internal standard solution (IS, 0.4 μg/mL of IT in methanol) was spiked. After high-speed centrifugation (14,000 rpm, 30 minutes), the supernatants were transferred into a glass tube and concentrated to dryness by a gentle steam of nitrogen at 40°C. Of the resulting sample, 10 μL was subjected to UPLC-MS/MS for assay.

Instrument parameters of UPLC-MS/MS

An Acquity-Xevo TQ system (Waters, USA) was used for UPLC-MS/MS analysis using positive electrospray ionization. The main parameters were as follows: source temperature 120°C, desolvation temperature 400°C, extractor 3 V, capillary 0.5 kV, cone 21 V, and nitrogen cone and desolvation gas flows of 50 and 750 L/h, respectively. Multiple reaction monitoring was used for the detection of CIT (retention time 1.70 minutes, m/z 369 → 313) and internal standard solution (retention time 1.20 minutes, m/z 369 → 313). Dwell time was set to 5 ms to ensure a minimum of ten data points per peak. Other mass parameters were optimized by analyzing individual standard solutions at a concentration of 20 mg/L.

An Acquity UPLC BEH C_{18} (1.7 µm, 2.1×50 mm; Waters) was used to complete separation. The column temperature was set at 30°C. The acetonitrile (A) and water (B, containing 0.1% formic acid) was the mobile phase of gradient elution. The gradient condition was: 0–1 minutes, 30% A; 1–2 minutes, linear from 30% to 80% A; 2–3 minutes, linear from 80% to 30% A; 3.0–3.5 minutes, held at 30% A for 30 seconds for equilibration of the column.

Statistical analysis

All values are expressed as means ± standard deviation, and were analyzed by one-way analysis of variance. A Student–Newman–Keuls post hoc test was conducted on the pooled data to determine the differences between the groups at a significance level of $P<0.05$.

Results

BMD

As shown in Table 1, the BMD of OVX rats significantly declined to 199.79±5.23 mg/cm^2 compared with 282.93±9.33 mg/cm^2 of the sham group ($P<0.01$). This showed that the OVX rats had decreased BMD of 29.37% after 12 weeks. Meanwhile, treatment with CIT at a dosage of 40 mg/kg (CIT-H) or 20 mg/kg (CIT-M) notably increased BMD by 13.6% ($P<0.01$) or 10.5% ($P<0.05$), respectively, compared with the OVX group. Likewise, the EV group also had increased BMD of 22.83% compared with OVX rats. Furthermore, the BMD of the CIT-SO-H and CIT-SO-M groups were higher than the CIT-H and CIT-M groups by 5.79% and 4.89%, respectively, and both differences were significant ($P<0.05$).

Trabecular bone structure

The quantitative results are expressed as BMC, TMC, TMD, VOB, Calib.Tb.Th.3D, CalibTbSp3D, BS/BV, BV/TV,

Table 1 BMD and other parameters of trabecular bone structures

Parameters	Sham	OVX	SO	EV	CIT-H	CIT-M	CIT-L	CIT-SO-H	CIT-SO-M	CIT-SO-L
BMD (mg/cm^2)	282.93±9.33^{b}	199.79±5.23	194.88±6.06	245.65±8.19^{a}	227.23±2.59^{b}	220.85±4.53^{a}	212.04±5.59	240.45±3.23^{b,d}	231.66±5.07^{a,c}	212.34±5.66
BMC (mg)	263.84±5.25^{b}	147.03±6.47	148.03±5.96	246.15±10.02^{b}	222.08±3.39^{b}	204.09±7.36^{b}	182.172±4.39^{b}	233.06±4.06^{b,f}	212.64±5.96^{b}	192.82±4.11^{b,e}
TMC (mg)	245.16±4.57^{b}	131.83±3.33	130.49±4.29	227.08±3.17^{b}	201.52±3.16^{b}	180.23±8.08^{b}	163.56±6.53^{b}	213.25±4.29^{b,f}	196.07±5.06^{b,c}	182.26±6.83^{b,e}
TMD (mg/cm^3)	587.37±2.92^{b}	488.14±4.62	483.15±1.87	579.00±4.77^{b}	554.44±7.37^{b}	515.86±5.49^{b}	509.87±0.10^{b}	576.74±4.27^{b,d}	535.26±4.89^{b,c}	523.01±4.22^{b,g}
VOB (mm^3)	448.08±16.78^{b}	241.25±17.07	237.26±15.03	415.75±12.94^{b}	382.53±8.98^{b}	358.19±10.16^{b}	312.46±17.31^{b}	409.60±13.06^{b,d}	389.99±10.59^{b,c}	347.79±11.05^{b,e}
CalibTbTh3D (mm)	0.76±0.04^{b}	0.44±0.04	0.42±0.05	0.67±0.01^{b}	0.61±0.02^{a}	0.57±0.01^{a}	0.50±0.01	0.64±0.01^{b,d}	0.59±0.01^{b,h}	0.55±0.01^{a,g}
CalibTbSp3D (mm)	0.22±0.01^{b}	0.58±0.01	0.60±0.02	0.30±0.01^{b}	0.35±0.02^{b}	0.42±0.01^{b}	0.53±0.01^{b}	0.31±0.01^{b,d}	0.36±0.02^{b,h}	0.49±0.01^{b,g}
BS/BV (1/mm)	2.71±0.09^{a}	5.44±0.11	5.49±0.14	3.41±0.05^{a}	3.77±0.07^{a}	4.06±0.08^{a}	4.55±0.09^{a}	3.68±0.06^{a,d}	3.87±0.04^{a,c}	4.19±0.07^{a,g}
BV/TV (%)	53.62±1.10^{a}	38.56±1.02	38.13±1.27	50.98±1.59^{a}	46.11±0.84^{a}	44.36±1.16^{a}	39.20±1.22^{a}	49.56±0.56^{a,f}	46.66±0.78^{a,c}	42.95±1.04^{a,e}
TbSp (mm)	0.24±0.01^{a}	0.69±0.03	0.70±0.02	0.32±0.01^{a}	0.41±0.02^{a}	0.45±0.01^{a}	0.61±0.01^{a}	0.34±0.01^{a,d}	0.40±0.01^{a,c}	0.54±0.02^{a}
TbTh (mm)	0.71±0.02^{a}	0.33±0.02	0.31±0.01	0.64±0.03^{a}	0.47±0.02^{a}	0.44±0.01^{a}	0.36±0.01^{a}	0.59±0.05^{a,d}	0.48±0.01^{a,c}	0.37±0.01^{a}
TbN (mm)	6.11±0.91^{a}	1.68±0.06	1.72±0.10	4.13±0.32^{a}	3.65±0.17^{a}	2.74±0.12^{a}	2.01±0.13^{a}	3.98±0.10^{a,d}	3.09±0.16^{a,c}	2.14±0.18^{a}

Notes: $^{a}P<0.05$ compared to OVX; $^{b}P<0.01$ compared to OVX; $^{c}P<0.05$ compared to CIT-M; $^{d}P<0.05$ compared to CIT-H; $^{e}P<0.05$ compared to CIT-L; $^{f}P<0.01$ compared to CIT-H; $^{g}P<0.01$ compared to CIT-L; $^{h}P<0.01$ compared to CIT-M. Data expressed as means ± standard deviation.

Abbreviations: BMD, bone mineral density; OVX, ovariectomized; SO, suet oil; EV, estradiol valerate; CIT, circinal–icaritin; H, high dosage; M, medium dosage; L, low dosage; BMC, BM content; TMC, tissue mineral content; TMD, TM density; VOB, volume of bone; CalibTbTh3D, calibration of trabecular thickness – 3-D; Sp, separation; BS/BV, bone surface over bone volume; TV, total volume; N, number.

TbSp, TbTh, and TbN in Table 1. The protective effect of CIT on microarchitecture and trabecular bone mass was enhanced with increasing doses, and was further demonstrated by 3-D micro-CT images (Figure 2). The OVX group showed conspicuous decrease in the trabecular area and TbN compared with the sham group. CIT inhibited bone loss induced by OVX, and significantly improved microarchitecture and trabecular bone mass. The morphometric parameters of distal femurs illustrated degeneration of the microarchitecture in the OVX rats compared with sham rats, which was evidenced by significant reductions in trabecular BMC, TMC, TMD, VOB, TbTh, BV/TV, TbN, and CalibTbTh3D ($P<001$) and significant increases in TbSp, BS/BV and CalibTbSp3D ($P<0.01$). Treatment with EV, CIT-H, CIT-M, CIT-SO-H, and CIT-SO-M reversed the aforementioned parameters, which were significant compared with the OVX group ($P<0.05$).

Compared with the CIT-H group, the CIT-SO-H group had significantly increased BMC (4.95%, $P<0.01$), TMC (5.97%, $P<0.01$), TMD (3.97%, $P<0.05$), VOB (7.07%, $P<0.05$), CalibTbTh3D (492%, $P<0.05$), BV/TV (761%, $P<0.01$), TbTh (2,553%, $P<0.05$), and TbN (904%, $P<0.05$), and significantly decreased CalibTbSp3D (1,143%, $P<0.05$), BS/BV (239%, $P<0.05$), and TbSp (1,707%, $P<0.05$). Compared with the CIT-M group, the CIT-SO-M group had significantly increased BMC (3.92%, $P<0.05$), TMC (8.89%, $P<0.05$), TMD (3.88%, $P<0.05$), VOB (8.66%, $P<0.05$), CalibTbTh3D (351%, $P<0.01$), BV/TV (455%, $P<0.05$), TbTh (909%, $P<0.05$), and TbN (1,278%, $P<0.05$), and significantly decreased BS/BV (468%, $P<0.05$) and TbSp (1,111%, $P<0.05$). Compared with the CIT-L group, the CIT-SO-L group had significantly increased BMC (5.49%, $P<0.05$), TMC (11.66%, $P<0.05$), TMD (2.75%, $P<0.01$), VOB (11.22%, $P<0.05$), Calib.TbTh3D (10.00%, $P<0.01$), and BV/TV (9.57%, $P<0.05$), and significantly decreased BS/BV (7.91%, $P<0.01$).

Bone biomechanical properties

The rats' biomechanical parameters after 12 weeks of treatment with CIT are shown in Table 2. After 12 weeks of estrogen deficiency, the biomechanical properties of tibias, such as energy absorption, stiffness, and ultimate load, showed a significant downward trend in the OVX rats compared with the sham rats ($P<0.01$).

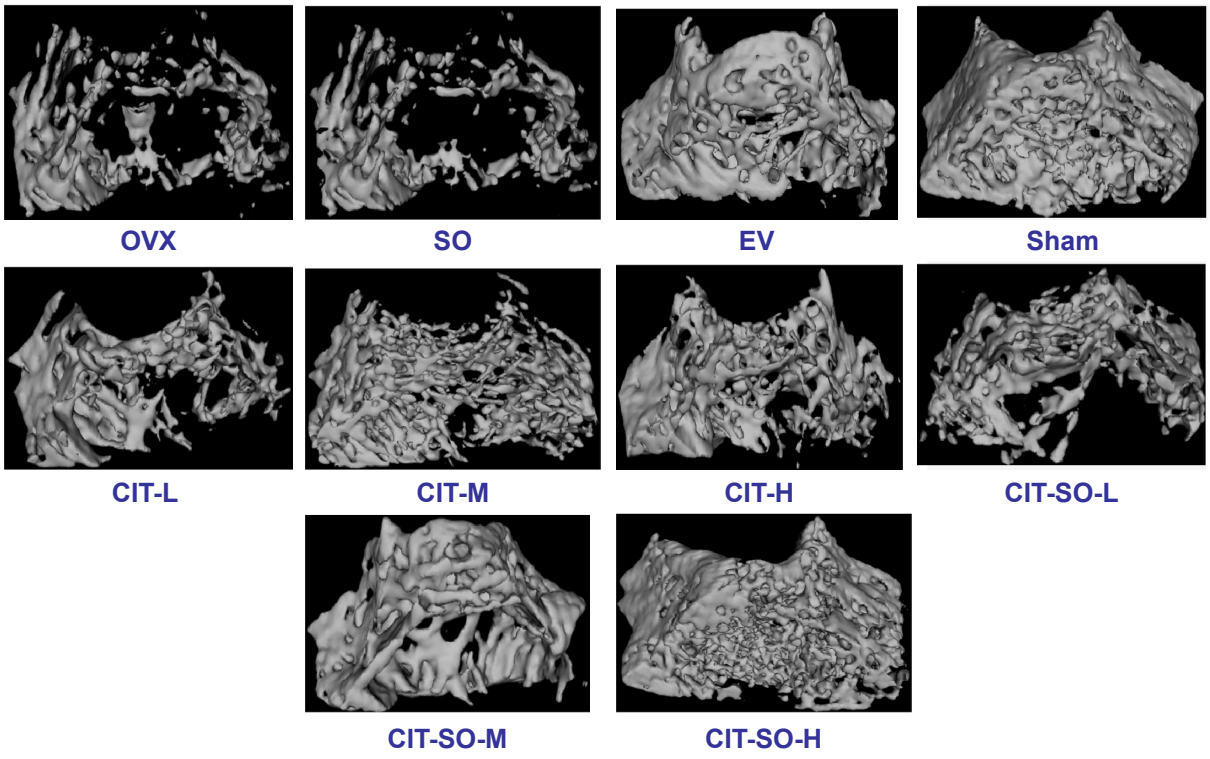

Figure 2 Representative micro-computed tomography images of trabecular bone microarchitecture in the distal femurs.
Notes: The OVX rats presented notable reductions in trabecular number and trabecular area compared with the sham rats. CIT, CIT-SO, and EV partially prevented OVX-induced trabecular bone loss and significantly improved trabecular bone mass and microarchitecture. CIT-SO significantly improved trabecular bone microarchitecture compared with CIT.
Abbreviations: OVX, ovariectomized; SO, suet oil; EV, estradiol valerate; CIT, circinal–icaritin; H, high dosage; M, medium dosage; L, low dosage.

Table 2 Bone biomechanical parameters by mechanical testing

Parameters	Sham	OVX	SO	EV	CIT-H	CIT-M	CIT-L	CIT-SO-H	CIT-SO-M	CIT-SO-L
Ultimate load (N)	94.66±3.99[b]	63.10567±2.69	60.11±5.67	88.76±1.72[b]	81.47±1.94[a,e]	76.10±1.57[a,d]	68.38±1.73[a]	87.26±2.91[b,e]	80.80±2.01[b,d]	72.16±1.56[b,c]
Stiffness (N/mm)	247.27±17.20[b]	146.29±12.33	143.62±9.68	224.02±6.38[b]	196.25±7.03[b,e]	177.48±8.53[a]	164.37±10.87	218.47±11.45[b,e]	197.08±7.65[b,d]	176.85±6.58[a]
Energy to failure (mJ)	23.37±2.02[b]	11.51±1.16	11.26±0.83	21.07±0.62[b]	18.92±0.47[b,e]	16.94±0.98[b,d]	13.99±1.00[a]	20.90±1.04[b,e]	19.16±0.83[b,d]	14.36±0.66[a]

Notes: [a]$P<0.05$ compared to OVX; [b]$P<0.01$ compared to OVX; [c]$P<0.05$ compared to CIT-L; [d]$P<0.05$ compared to CIT-M; [e]$P<0.05$ compared to CIT-H. Data expressed as means ± standard deviation.

Abbreviations: OVX, ovariectomized; SO, suet oil; EV, estradiol valerate; CIT, circinal–icaritin; H, high dosage; M, medium dosage; L, low dosage.

Biomechanical strength was significant increased after EV, CIT-H, CIT-M, CIT-SO-H, and CIT-SO-M treatment compared with the OVX group ($P<0.05$), which was demonstrated by increased levels of energy absorption, stiffness, and ultimate load. Moreover, compared with the CIT-H group, energy to failure, stiffness, and ultimate load of the CIT-SO-H group were increased by 11.11% ($P<0.05$), 11.22% ($P<0.05$), and 7.41% ($P<0.05$), respectively. Energy to failure, stiffness, and ultimate load of the CIT-SO-M group were increased by 18.75% ($P<0.05$), 11.29% ($P<0.05$), and 5.26% ($P<0.05$), respectively, compared with the CIT-M group, while the ultimate load of the CIT-SO-L group increased by 5.88% ($P<0.05$).

Bone-turnover markers in serum

The effects of CIT on serum biochemical markers of osteoporosis rats after 12 weeks of treatment are shown in Figure 3. The OVX group showed significant increases ($P<0.01$) in serum HOP, ALP, TRACP-5b, and RANKL by 34.33%, 199.78%, 77.22%, and 99.29%, respectively, compared with the sham group. Treatment with EV, CIT-H, CIT-M, CIT-L, CIT-SO-H, CIT-SO-M, and CIT-SO-L differentially prevented the elevation of serum HOP, ALP, TRACP-5b, and RANKL levels compared with the OVX group. Meanwhile, OVX rats showed significantly decreased ($P<0.01$) levels of serum OPG and OCN by 38.09% and 45.27%, respectively, compared with the sham group. Treatment with EV, CIT-H, CIT-M, CIT-L, CIT-SO-H, CIT-SO-M, and CIT-SO-L differentially increased the elevation of serum OPG and OCN levels compared with the OVX group.

The serum HOP, ALP, TRACP-5b, and RANKL of the CIT-SO-H group were decreased by 3.51% ($P<0.05$), 5.26% ($P<0.05$), 9.81% ($P<0.01$), and 3.13% ($P<0.05$), respectively, compared with CIT-H. The serum HOP, ALP, TRACP-5b, and RANKL of the CIT-SO-M group were decreased by 3.14% ($P<0.05$), 6.82% ($P<0.05$), 9.81% ($P<0.01$), and 3.86% ($P<0.05$), respectively, compared with CIT-M. The serum HOP, ALP, TRACP-5b, and RANKL of the CIT-SO-L group were decreased by 3.85% ($P<0.05$), 8.33% ($P<0.05$), 1.88% ($P<0.01$), and 11.91% ($P<0.01$), respectively, compared with CIT-L. Compared with the CIT-H group, the serum OPG and OCN of the CIT-SO-H group was higher: these increased by 2.65% ($P<0.05$), and 14.58% ($P<0.05$), respectively. Compared with the CIT-M group, the serum OPG and OCN of the CIT-SO-M group were higher: these increased by 5.56% ($P<0.05$) and 14.63% ($P<0.01$), respectively. Compared with the CIT-L group, the OPG and OCN of the CIT-SO-L group were higher:

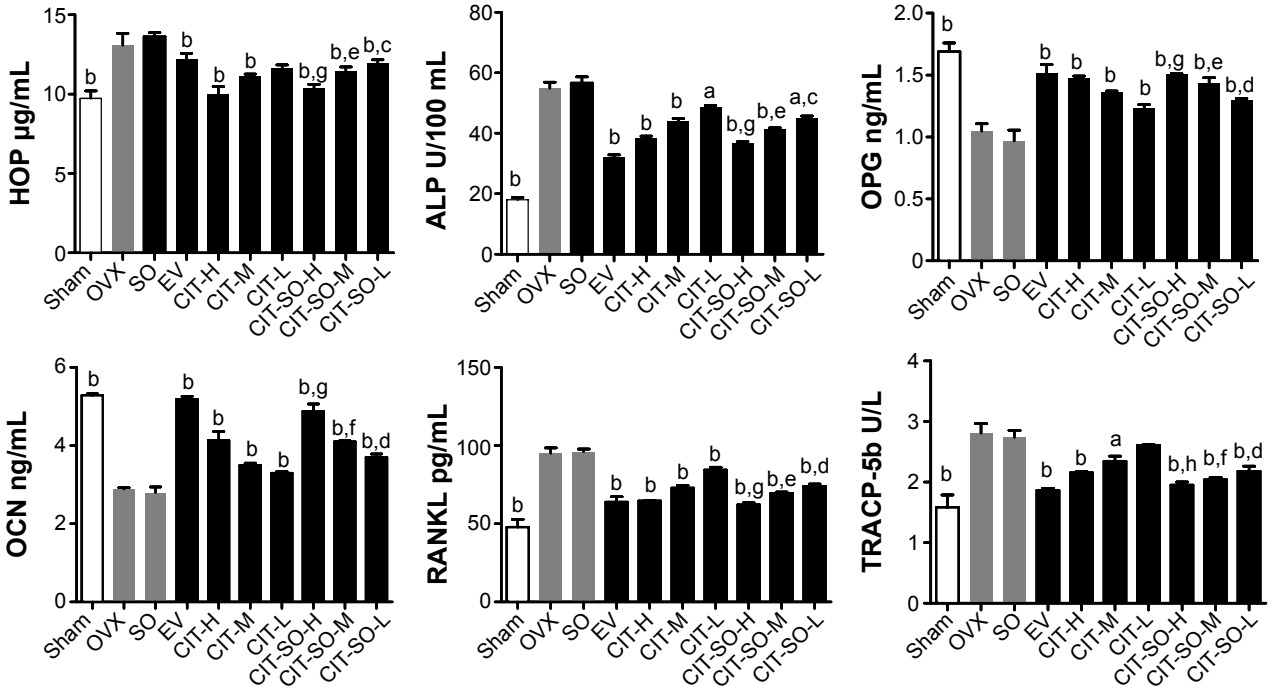

Figure 3 Serum parameters changes in the OVX model of osteoporosis.

Notes: [a]$P<0.05$ compared to OVX; [b]$P<0.01$ compared to OVX; [c]$P<0.05$ compared to CIT-L; [d]$P<0.01$ compared to CIT-L; [e]$P<0.05$ compared to CIT-M; [f]$P<0.01$ compared to CIT-M; [g]$P<0.05$ compared to CIT-H; [h]$P<0.01$ compared to CIT-H.

Abbreviations: OVX, ovariectomized; SO, suet oil; EV, estradiol valerate; CIT, circinal–icaritin; H, high dosage; M, medium dosage; L, low dosage; HOP, hydroxyproline; ALP, alkaline phosphatase; OPG, osteoprotegerin; OCN, osteocalcin; RANKL, receptor activator of nuclear factor-κB ligand; TRACP-5b, tartrate-resistant acid phosphatase 5b.

these increased by 5.38% ($P<0.01$) and 8.33% ($P<0.01$), respectively.

Expressions of OPG and RANKL

The protein expressions of OPG and RANKL are shown in Figure 4A, and the messenger RNA (mRNA) expressions of OPG and RANKL are shown in Figure 4B. Protein and mRNA expressions of OPG were decreased significantly in the OVX group compared with the sham group ($P<0.01$). Treatment with EV, CIT-H, CIT-M, CIT-L, CIT-SO-H, CIT-SO-M, and CIT-SO-L increased OPG protein and mRNA expressions compared with the OVX group. Protein and mRNA expressions of RANKL significantly increased after ovariectomy compared with the sham group ($P<0.01$). RANKL protein or mRNA expressions of OVX rats decreased significantly after EV, CIT-H, CIT-M, CIT-L, CIT-SO-H, CIT-SO-M, and CIT-SO-L treatment. Furthermore, the CIT-SO-H treatment group had significantly decreased RANKL protein ($P<0.05$) and mRNA ($P<0.01$) expressions, and significantly increased OPG protein ($P<0.05$) and mRNA ($P<0.05$) expressions compared with the CIT-H group. The CIT-SO-M treatment group had significantly decreased RANKL protein ($P<0.05$) and mRNA ($P<0.05$) expressions, and significantly increased OPG mRNA ($P<0.05$) expressions compared with the CIT-M group. CIT-SO-L decreased the RANKL protein ($P<0.05$) and mRNA ($P<0.01$) expressions compared with the CIT-L group.

In vivo pharmacokinetic studies

The pharmacokinetic parameters of CIT and CIT-SO are displayed in Table 3 and Figure 5. After oral administration, the average maximum concentration (C_{max}) of CIT-H, CIT-M, and CIT-L was 56.72, 26.11, and 14.16 μg/L, respectively. However, the average value of C_{max} of CIT-SO-H, CIT-SO-M, and CIT-SO-L was 64.38 μg/L, 31.56 μg/L, and 18.98 μg/L, respectively, which all were significantly different compared with the CIT groups ($P<0.01$). This indicated that SO increased the absorption of CIT. The average area under the curve from 0 to infinity ($AUC_{0-\infty}$) of CIT-H, CIT-M, CIT-L were 680.40, 313.20, and 171.34 mg/L per hour, respectively. The $AUC_{0-\infty}$ values of CIT-SO-H, CIT-SO-M, and CIT-SO-L were 751.54, 335.55, and 204.31 mg/L per hour, respectively. The $AUC_{0-\infty}$ values of CIT-SO-H, CIT-SO-M, and CIT-SO-L were significantly higher than that of CIT-H (1.27 times, $P<0.01$), CIT-M (1.20 times, $P<0.01$), and CIT-L (1.35 times, $P<0.01$).

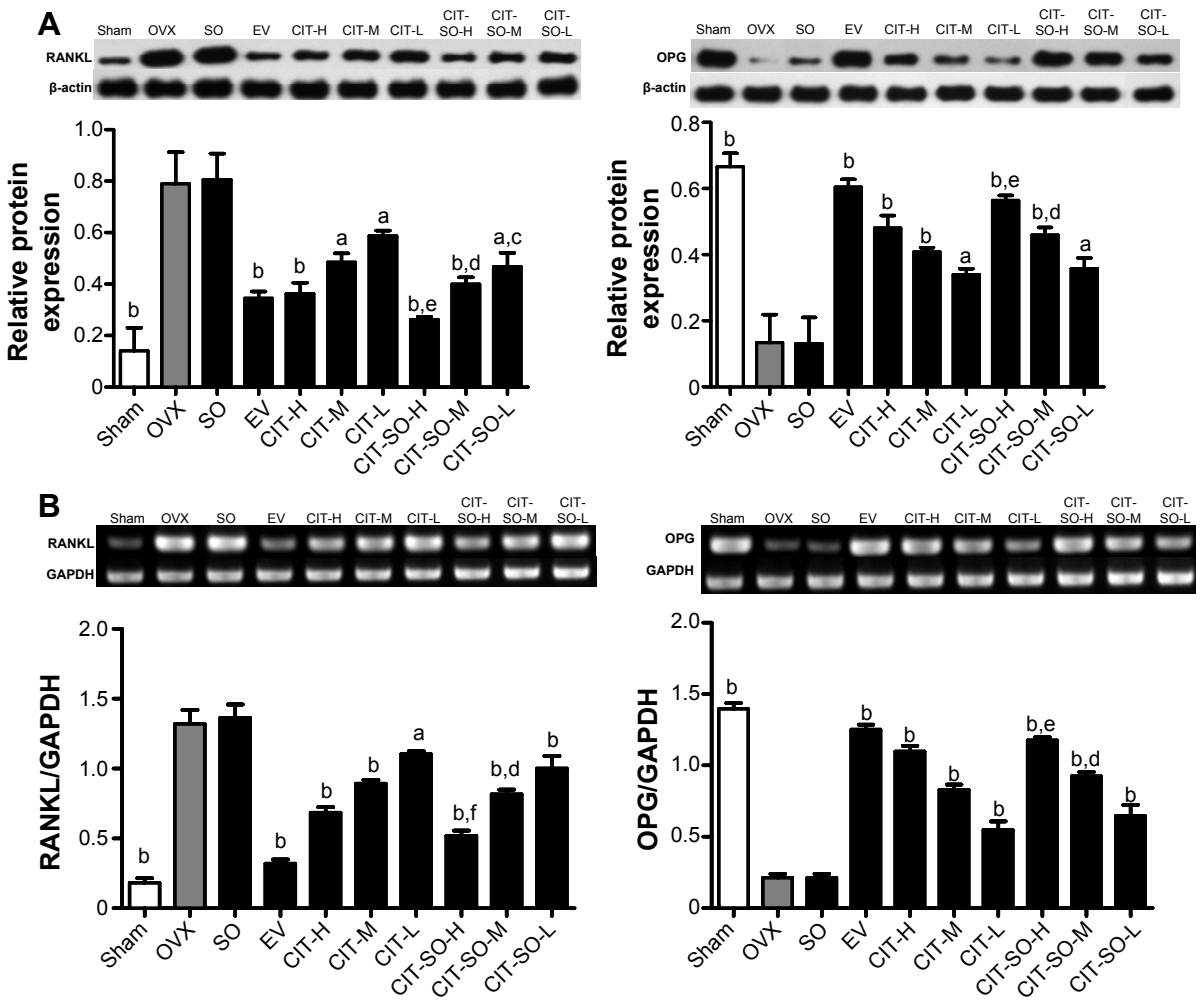

Figure 4 Related protein and gene expressions in osteoporotic rat femurs.

Notes: (**A**) OPG and RANKL protein expressions in femurs of OVX rats. Effects of 12-week treatment with EV, CIT-H, CIT-M, CIT-L, CIT-SO-H, CIT-SO-M, and CIT-SO-L on protein expressions of OPG and RANKL. (**B**) OPG and RANKL mRNA expressions in femur of OVX rats treated with EV, CIT-H, CIT-M, CIT-L, CIT-SO-H, CIT-SO-M, and CIT-SO-L for 12 weeks. Total RNA was isolated, and reverse-transcription polymerase chain reaction was performed to determine OPG and RANKL mRNA expressions. Values are expressed as means ± standard deviation (n=8); $^{a}P<0.05$ compared to OVX, $^{b}P<0.01$ compared to OVX, $^{c}P<0.05$ compared to CIT-L, $^{d}P<0.05$ compared to CIT-M, $^{e}P<0.05$ compared to CIT-H, $^{f}P<0.01$ compared to CIT-H.

Abbreviations: OVX, ovariectomized; SO, suet oil; EV, estradiol valerate; CIT, circinal–icaritin; H, high dosage; M, medium dosage; L, low dosage; RANKL, receptor activator of nuclear factor-κB ligand; OPG, osteoprotegerin; mRNA, messenger ribonucleic acid; OCN, osteocalcin; GAPDH, glyceraldehyde 3-phosphate dehydrogenase.

Size distribution of self-assembled nanomicelles

The size distributions of the self-prepared CIT-DOC and CIT-DOC-SO are displayed in Table 4. The average particle size and polydispersity of the CIT-DOC group were 204.77±6.81 nm and 0.36±0.02, respectively. Compared with the CIT-DOC group, the CIT-DOC-SO group had a significantly reduced size distribution of about 0.30±0.02 polydispersity ($P<0.05$), and a significantly reduced average particle size of about 100.80±7.21 nm ($P<0.01$), as shown in Figure 6A and B. Consequently, this implied that the particle size and size distribution of CIT-DOC was smaller and stabler under the action of SO, which significantly affected the formation of self-assembled micelles.

The CIT-DOC-SO self-assembled nanomicelles seemed to be monodisperse spherical particles with a smooth surface, determined by TEM (Figure 6C and D). Meanwhile, the CIT-DOC-SO self-assembled nanomicelles had smaller average particle size than CIT-DOC. The TEM images further confirmed the particle size detected by dynamic light scattering.

Intestinal absorption of CIT-DOC and CIT-DOC-SO

The P*eff values of CIT-DOC and CIT-DOC-SO in different segments are displayed in Figure 7. The permeability values of CIT-DOC in the duodenum, jejunum, ileum, and colon were 0.49±0.01 10-4 cm/s, 0.48±0.01, 0.39±0.01, and 0.36±0.01,

Table 3 Pharmacokinetic parameters of CIT and CIT-SO administered orally to rats (n=3)

Parameters	CIT-H	CIT-M	CIT-L	CIT-SO-H	CIT-SO-M	CIT-SO-L
AUC_{0-t} (mg/L per hour)	607.75±3.16	279.54±7.46	151.44±19.65	751.54±32.90**	335.55±9.16##	204.31±3.56Δ
$AUC_{0-\infty}$ (mg/L per hour)	680.40±2.61	313.20±8.00	171.34±22.98	865.31±38.98**	379.09±10.13##	229.56±1.90Δ
MRT_{0-t} (hours)	12.11±0.17	12.23±0.05	12.23±0.03	12.83±0.23*	12.20±0.05	12.16±0.04
$MRT_{0-\infty}$ (hours)	16.79±0.49	16.90±0.09	17.43±0.38	18.63±0.31**	17.35±0.13##	17.00±0.54
$t_{1/2}$ (hours)	12.92±0.42	12.88±0.15	13.55±0.42	13.56±0.53**	13.54±0.13##	13.15±0.63
Cl (L/h/kg)	59.03±0.90	127.77±3.31	236.08±2.94	46.29±2.14**	105.57±2.85##	174.26±1.45Δ
C_{max} (μg/L)	56.72±0.62	26.11±0.53	14.16±1.90	64.38±0.43**	31.56±0.86##	18.98±0.42Δ

Notes: *$P<0.05$, **$P<0.01$ compared with CIT-H group; ##$P<0.01$ compared with CIT-M group; Δ$P<0.05$ compared with CIT-L group. Data expressed as means ± standard deviation.

Abbreviations: CIT, circinal–icaritin; SO, suet oil; H, high dosage; M, medium dosage; L, low dosage; AUC, area under the curve; MRT, mean residence time; $t_{1/2}$, half-life; Cl, clearance; C_{max}, maximum concentration.

respectively. The permeability values of CIT-DOC-SO in the duodenum, jejunum, ileum, and colon were 0.94±0.08, 0.90±0.07, 0.88±0.06, and 0.87±0.06, respectively. According to our results, the CIT-DOC-SO group had significantly increased P*eff values in the duodenum, jejunum, ileum, and colon ($P<0.01$) compared with the CIT-DOC group. Therefore, the CIT-DOC-SO self-assembled nanomicelles improved the P*eff value of CIT under the action of SO, which promoted the intestinal absorption of CIT.

Discussion

Estrogen deficiency is one of the main reasons for the occurrence and development of osteoporosis. Ovariectomy leads to a significant reduction in uterine and femur weight, bone quality, BMD, and biomechanical strength, attributed to estrogen deficiency.[31] The RANKL/RANK/OPG system is an important factor in the regulation of bone remodeling.[32] RANK is a receptor located on the surface of osteoclasts. Ligands of RANK are OPG- and RANKL-synthesized and secreted primarily by osteoblasts and bone marrow stromal cells.[33] When RANK is activated by the RANKL, a signaling cascade is initiated, causing osteoclast differentiation and increased bone resorption. OPG, which acts as a decoy receptor for RANKL, blocks this interaction. Therefore, OPG and RANKL are two important indicators that are directly related to osteoporosis.

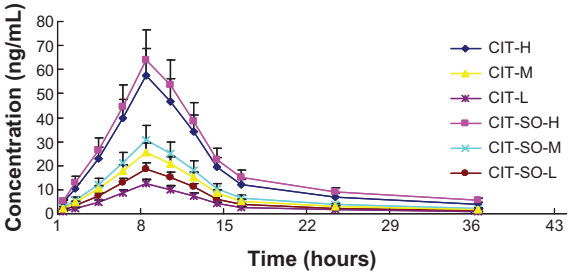

Figure 5 The plasma concentration–time curve of CIT in rats after oral administration of CIT and CIT-SO.

Notes: Dosage 40 mg/kg for CIT-H and CIT-SO-H, 20 mg/kg for CIT-M and CIT-SO-M, and 10 mg/kg for CIT-L and CIT-SO-L.

Abbreviations: CIT, circinal–icaritin; SO, suet oil; H, high dosage; M, medium dosage; L, low dosage.

Previous studies have shown that total flavonoids of *Epimedium* had no significantly acute toxicity or long-term toxicity at doses of 36 g/kg/day for 7 days (equal to 1,440 times the normal human dosage) and 410 g/kg/day for 12 weeks. CIT is one of the main total flavonoids of *Epimedium*.[34] Therefore, CIT has good safety and few side effects at a relatively high dose. High, medium, and low dosages of CIT were respectively 40, 20, and 10 mg/kg body weight/day, which are equivalent to an adult (60 kg body weight) at doses of 0.48, 0.24, and 0.12 g/kg body weight/day.

SO enhanced the antiosteoporotic effects of CIT, and can be summarized as follows: 1) protein and mRNA expressions of OPG increased, while the protein and mRNA expressions of RANKL decreased in bone tissue; 2) bone-turnover markers in serum HOP, ALP, TRACP-5b, and RANKL levels decreased, while OPG and OCN levels increased; and 3) trabecular bone mass, microarchitecture, and bone biomechanical strength were enhanced. These three points demonstrate that the participation of SO indeed exerted a synergistic role to enhance the antiosteoporosis effect of CIT.

SO contains abundant unsaturated fatty acids and saturated fatty acids. Our previous study found that there were 25 kinds of fatty acids in SO distributed widely from

Table 4 Physicochemical properties of CIT with or without SO

Groups	Average size (nm)	Polydispersity
CIT-DOC	204.77±6.81	0.36±0.02
CIT-DOC-SO	100.80±7.21[a]	0.30±0.02[b]

Notes: [a]$P<0.01$ compared with average size of CIT-DOC group; [b]$P<0.05$ compared with polydispersity of CIT-DOC group. Data expressed as means ± standard deviation.

Abbreviations: CIT, circinal–icaritin; SO, suet oil; DOC, sodium deoxycholate.

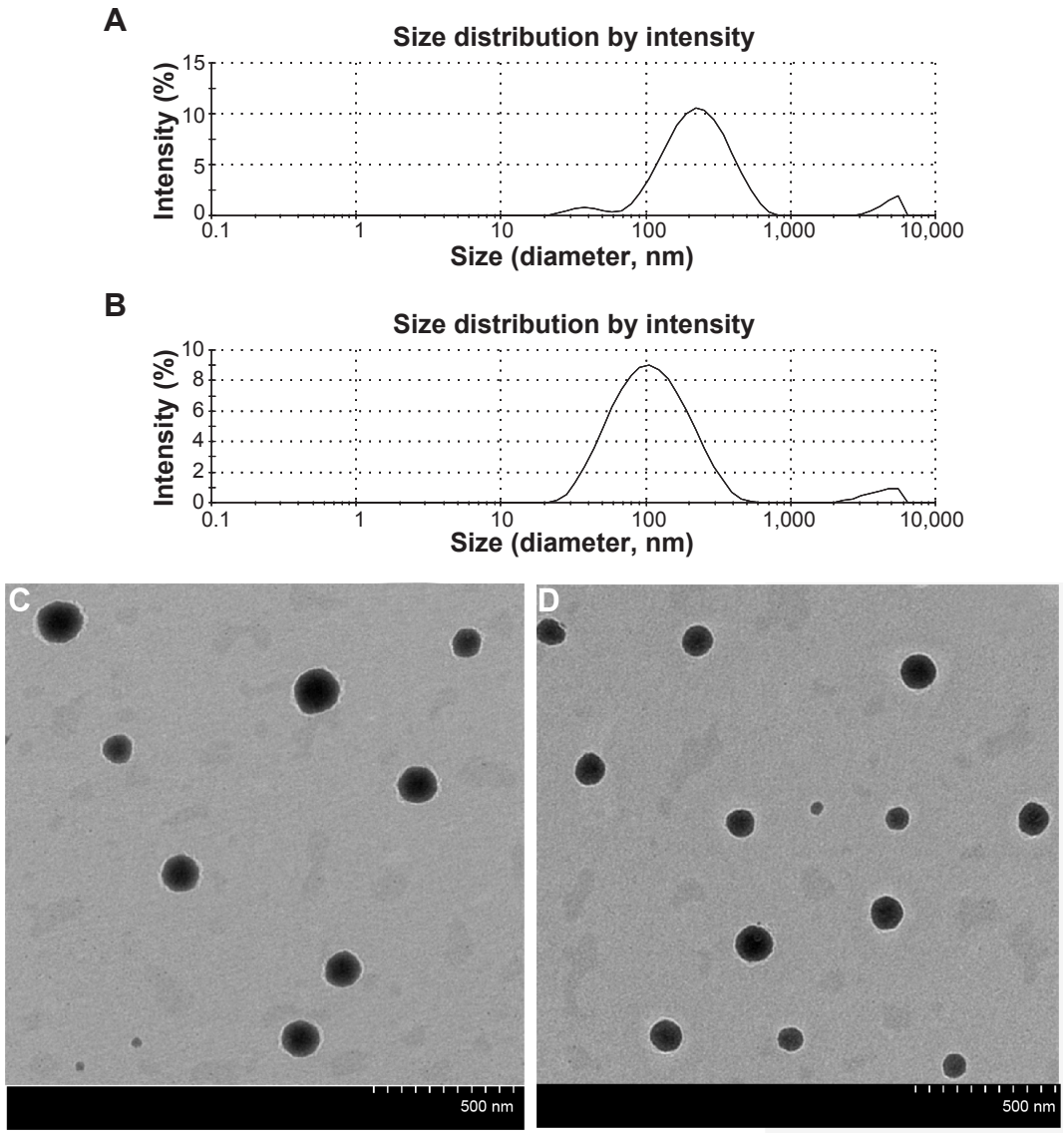

Figure 6 Particle-size distribution and transmission electron microscopy of CIT-DOC and IT-SO-DOC.
Notes: (**A**) Particle-size distribution of CIT-DOC; (**B**) particle-size distribution of CIT-SO-DOC; (**C**) transmission electron microscopy of CIT-DOC; (**D**) transmission electron microscopy of CIT-SO-DOC. The average size of CIT-SO-DOC micelle was 100.80±7.21 nm, which was significantly lower than the 204.77±6.81 nm of the CIT-DOC group. The CIT-SO-DOC self-assembled nanomicelles seemed to be monodisperse spherical particles with smooth surfaces.
Abbreviations: CIT, circinal–icaritin; DOC, sodium deoxycholate; SO, suet oil.

12 to 20 carbons, in which oleic acid, hexadecanoic acid and octadecanoic acid were the main ingredients.[7] The properties of these fatty acids are similar to surfactants, which are helpful for the preparation of nanomicelles.[16–20] In the human body, the inherent bile acids or their salts have hydrophilic and hydrophobic surfaces, which are natural biosurfactants. Bile-acid salts can form nanomicelles with phospholipids, glycerides, fatty acids, and other surfactants as drug carriers, and promote drug absorption.[35–37] The abundant fatty acids contained in SO have long chains and surface activity, which can form self-assembled nanomicelles together with the role of bile salts in the body. Therefore, the self-assembled nanomicelles are carriers that improve the absorption of CIT and have a synergistic effect against osteoporosis.

It was found that the average particle size of CIT significantly decreased after adding SO, which promoted CIT-SO self-assembled nanomicelle stability. An intestinal absorption experiment indicated that the CIT-SO self-assembled micelles improved the P*eff value of CIT and promoted intestinal absorption.

Conclusion

SO promoted the formation of CIT-SO-DOC self-assembled nanomicelles, which reduced the particle size, increased

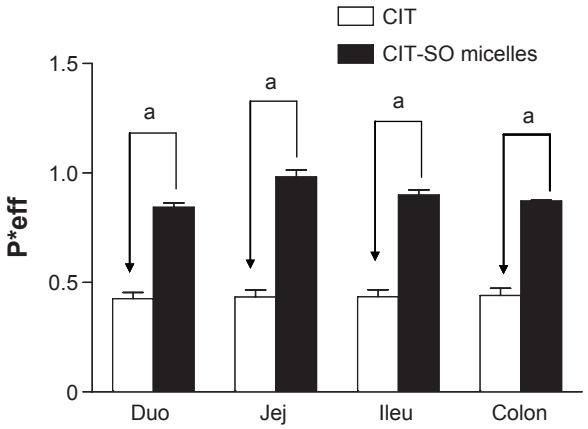

Figure 7 The permeability-coefficient (P*eff) values of CIT and CIT-SO in the duodenum (Duo), jejunum (Jej), ileum (Ileu), and colon.
Notes: [a]$P<0.01$ compared with CIT-DOC group. Data expressed as means ± standard deviation (n=4).
Abbreviations: CIT, circinal–icaritin; SO, suet oil.

solubility, promoted intestinal absorption, and improved the bioavailability of CIT. The CIT-SO-DOC self-assembled nanomicelles had a diameter of 100.80±7.21 nm. The results of rat intestinal perfusion and pharmacokinetic studies suggested increased CIT absorption in vivo. Further, the results of a pharmacokinetic study in rats showed that the relative bioavailability values of CIT-SO-H, CIT-SO-M, and CIT-SO-L ($AUC_{0-\infty}$) compared with that of raw CIT-H, CIT-M, CIT-L ($AUC_{0-\infty}$) were 127%, 121%, and 134%, respectively. SO is a practical oral carrier for anti-osteoporosis drugs with low bioavailability.

Acknowledgment

This work was supported by the Natural Science Foundation of China (81274088).

Disclosure

The authors report no conflicts of interest in this work.

References

1. Gao SG, Cheng L, Li KH, et al. Effect of *Epimedium pubescen* flavonoid on bone mineral status and bone turnover in male rats chronically exposed to cigarette smoke. *BMC Musculoskelet Disord*. 2012;13:105.
2. Zhai YK, Guo X, Pan YL, et al. A systematic review of the efficacy and pharmacological profile of Herba Epimedii in osteoporosis therapy. *Pharmazie*. 2013;68:713–722.
3. Xu YX, Wu CL, Wu Y, et al. *Epimedium*-derived flavonoids modulate the balance between osteogenic differentiation and adipogenic differentiation in bone marrow stromal cells of ovariectomized rats via Wnt/β-catenin signal pathway activation. *Chin J Integr Med*. 2012;18:909–917.
4. Deng WM, Zhang P, Huang H, et al. Five-year follow-up study of a kidney-tonifying herbal fufang for prevention of postmenopausal osteoporosis and fragility fractures. *J Bone Miner Metab*. 2012;30:517–524.
5. Peng S, Zhang G, He Y, et al. *Epimedium*-derived flavonoids promote osteoblastogenesis and suppress adipogenesis in bone marrow stromal cells while exerting an anabolic effect on osteoporotic bone. *Bone*. 2009;45:534–544.
6. Jiang J, Feng L, Sun E, Li H, Cui L, Jia X. Metabolic profiling of isomeric aglycones central-icaritin (c-IT) and icaritin (IT) in osteoporotic rats by UPLC-QTOF-MS. *Drug Test Anal*. Epub 2014 Jun 16.
7. Jiang J, Jia XB. Profiling of fatty acids composition in suet oil based on GC-EI-qMS and chemometrics analysis. *Int J Mol Sci*. 2014;15.
8. Cui L, Sun E, Qian Q, Fan HW, Zou JJ, Jia XB. [Comparative study on effect of crude and different processed products of *Epimedium* on pharmacokinetics characteristics in mice]. *Zhongguo Zhong Yao Za Zhi*. 2013;38:1614–1617. Chinese.
9. Sun E, Wei YJ, Zhang ZH, Cui L, Xu FJ, Jia XB. [Processing mechanism of *Epimedium* fried with suet oil based on absorption and metabolism of flavonoids]. *Zhongguo Zhong Yao Za Zhi*. 2014;39:383–390. Chinese.
10. Sun E, Zhang ZH, Cui L, Xu FJ, Li J, Jia XB. [Discussion on research ideas of synergistic mechanism of *Epimedium* fried with suet oil based on self-assembled micelles formation in vivo]. *Zhongguo Zhong Yao Za Zhi*. 2014;39:378–382. Chinese.
11. Hofmann AF, Hagey LR. Key discoveries in bile acid chemistry and biology and their clinical applications: history of the last eight decades. *J Lipid Res*. 2014;55:1553–1595.
12. Dong F, Xie Y, Qi J, et al. Bile salt/phospholipid mixed micelle precursor pellets prepared by fluid-bed coating. *Int J Nanomedicine*. 2013;8:1653–1663.
13. Mahajan S, Mahajan RK. Interactions of phenothiazine drugs with bile salts: micellization and binding studies. *J Colloid Interface Sci*. 2012;387:194–204.
14. van Hasselt PM, Janssens GE, Rijcken CJ, van Nostrum CF. Influence of bile on the oral bioavailability of vitamin K-loaded polymeric micelles. *J Control Release*. 2008;132:29–31.
15. Jiang L, Wang K, Deng M, Wang Y, Huang J. Bile salt-induced vesicle-to-micelle transition in catanionic surfactant systems: steric and electrostatic interactions. *Langmuir*. 2008;24:4600–4606.
16. Narayanan VS, Storch J. Fatty acid transfer in taurodeoxycholate mixed micelles. *Biochemistry*. 1996;35:7466–7473.
17. Turner DC, Yin F, Kindt JT, Zhang H. Molecular dynamics simulations of glycocholate-oleic acid mixed micelle assembly. *Langmuir*. 2010;26:4687–4692.
18. Schwarz MA, Raith K, Dongowski G, Neubert RH. Effect on the partition equilibrium of various drugs by the formation of mixed bile salt/phosphatidylcholine/fatty acid micelles. A characterization by micellar affinity capillary electrophoresis. Part IV. *J Chromatogr A*. 1998;809:219–229.
19. Hashizume M, Douen T, Murakami M, Yamamoto A, Takada K, Muranishi S. Improvement of large intestinal absorption of insulin by chemical modification with palmitic acid in rats. *J Pharm Pharmacol*. 1992;44:555–559.
20. Devraj R, Williams HD, Warren DB, Mullertz A, Porter CJ, Pouton CW. In vitro digestion testing of lipid-based delivery systems: calcium ions combine with fatty acids liberated from triglyceride rich lipid solutions to form soaps and reduce the solubilization capacity of colloidal digestion products. *Int J Pharm*. 2013;441:323–333.
21. Pisani P, Renna MD, Conversano F, et al. Screening and early diagnosis of osteoporosis through X-ray and ultrasound based techniques. *World J Radiol*. 2013;28;5:398–410.
22. Peng S, Zhang G, Zhang BT, et al. The beneficial effect of icaritin on osteoporotic bone is dependent on the treatment initiation timing in adult ovariectomized rats. *Bone*. 2013;55:230–240.
23. Peng Z, Tuukkanen J, Zhang H, Jämsä T, Väänänen HK. The mechanical strength of bone in different rat models of experimental osteoporosis. *Bone*. 1994;15:523–532.
24. Jagtap VR, Ganu JV. Effect of antiresorptive therapy on urinary hydroxyproline in postmenopausal osteoporosis. *Indian J Clin Biochem*. 2012;27:90–93.

25. Ornstrup MJ, Harsløf T, Kjær TN, Langdahl BL, Pedersen SB. Resveratrol increases bone mineral density and bone alkaline phosphatase in obese men: a randomized placebo-controlled trial. *J Clin Endocrinol Metab*. 2014;99:4720–4729.
26. Titanji K, Vunnava A, Sheth AN, et al. Dysregulated B cell expression of RANKL and OPG correlates with loss of bone mineral density in HIV infection. *PLoS Pathog*. 2014;10:e1004497.
27. Yeap BB, Alfonso H, Paul Chubb SA, et al. Higher serum undercarboxylated osteocalcin and other bone turnover markers are associated with reduced diabetes risk and lower estradiol concentrations in older men. *J Clin Endocrinol Metab*. Epub 2014 Nov 3.
28. Jiang J, Li J, Jia X. The antiosteoporotic activity of central-icaritin (CIT) on bone metabolism of ovariectomized rats. *Molecules*. 2014; 19:18690–18704.
29. Chmielnicka M, Woźniacka A, Torzecka JD. The influence of corticosteroid treatment on the OPG/RANK/RANKL pathway and osteocalcin in patients with pemphigus. *Postepy Dermatol Alergol*. 2014;31: 281–288.
30. Laib A, Kumer JL, Majumdar S, Lane NE. The temporal changes of trabecular architecture in ovariectomized rats assessed by micro CT. *Osteoporos Int*. 2001;12:936–941.
31. Nian H, Ma MH, Nian SS, Xu LL. Antiosteoporotic activity of icariin in ovariectomized rats. *Phytomedicine*. 2009;16:320–326.
32. Boyce BF, Xing L. Functions of RANKL/RANK/OPG in bone modeling and remodeling. *Arch Biochem Biophys*. 2008;473:139–146.
33. Kobayashi Y, Udagawa N, Takahashi N. Action of RANKL and OPG for osteoclastogenesis. *Crit Rev Eukaryot Gene Expr*. 2009;19:61–72.
34. Ma H, He X, Yang Y, et al. The genus *Epimedium*: an ethnopharmacological and phytochemical review. *J Ethnopharmacol*. 2011; 134:519–541.
35. Tengamnuay P, Mitra AK. Bile salt-fatty acid mixed micelles as nasal absorption promoters of peptides. I. Effects of ionic strength, adjuvant composition, and lipid structure on the nasal absorption of [D-Arg2] kyotorphin. *Pharm Res*. 1990;7:127–133.
36. Zhao Y, Cui Y, Li Y, Li L. Stable phosphatidylcholine-bile salt mixed micelles enhance oral absorption of paclitaxel: preparation and mechanism in rats. *J Drug Target*. 2014;31:1–12.
37. Jin S, Fu S, Han J, et al. Improvement of oral bioavailability of glycyrrhizin by sodium deoxycholate/phospholipid-mixed nanomicelles. *J Drug Target*. 2012;20:615–622.